MEASUREMENT OF SITE SPECIFIC BINDING ENERGY OF SURFACE ATOMS

Y. Liou, T. Tsong

JOURNAL DE PHYSIQUE
Colloque C6, supplément au n°11, Tome 49, novembre 1988

MEASUREMENT OF SITE SPECIFIC BINDING ENERGY OF SURFACE ATOMS

Y. LIOU and T.T. TSONG

Physics Department, The Pensylvania State University, University Park, Pennsylvania, PA 16802, U.S.A.

Abstract - The binding energies of kink site surface atoms have been determined from a measurement of ion energy distribution in low temperature field evaporation. With improvements in both the electronic and vacuum systems, and elaborate calibrations, the high-resolution pulsed-laser time-of-flight atom-probe has achieved an energy resolution of one part over 50000, just adequate for this study. The binding energy of pure metals such as Rh or W can be measured at well defined crystal planes and sitesat low temperatures. We find that the cohesive energy of metals measured with thermodynamic method is equal to the binding energy of kink site atoms. For instance, the binding energy of kink site atoms at Rh(100) surface, or at W(110) surface, is the same as the cohesive energy of Rh ,or W listed in standard tables. For compound materials, such as PtRh alloy or GaAs, surface atoms of different kinds have different binding energies which are different from those of the pure elements. We measure the binding energy of Pt and Rh from the surface of PtRh, and of Ga from the surface of GaAs.

1. INTRODUCTION

The study of binding energy of atoms or the atomic bonds on surfaces and cohesive energy of solids is one of the fundamental topics in condensed matter physics[1]. We report here a measurement of the site specific binding energy of atoms on solid surfaces using low temperature field evaporation, at temperatures below 100 K, where the surface atomic structure remains unchanged; thus atoms are removed from well defined atomic sites. The cohesive energy in the crystal bulk is defined as the energy difference between the free atom energy and the crystal energy. Based on the pair potential calculation, without considering the surface effect, the cohesive energy of an atom in the bulk is equal to one half of the total pair potential energy of this atom[2]. On crystal surfaces, atoms of different sites have variable numbers of nearest neighbors. The atom at the kink site is most significant because the corrdination numbers are exactly equal to one half of those of a bulk atom. So the binding energy of the kink site atom should be equal to the cohesive energy. In field evaporation of lattice atoms on the crystal planes, the atoms come from the kink sites at the lattice steps of the surface[3].

The critical energy deficit in the energy distribution of field emitted ions is related to the binding energy of the surface atoms. The critical energy deficit is determined by measuring the onset flight time of the time-of-flight distribution which is also the energy distribution. By using the newly improved pulsed-laser time-of-flight atom-probe, with an energy resolution of better than 1/50000, we have measured the critical energy deficit of field emitted ions. But without an elaborate calibration of the system, the measurement can not be reliable. So a very careful calibration has been done and the system constants have been accurately determined. Precision measurements of ionic masses and critical energy deficits of gas and metal ions also have been done to test the accuracy of the calibration.

Experiments of measuring critical energy deficit for pure metals such as Rh and W, an alloy of Pt-Rh and a compound semiconductor GaAs have been done. The binding energy of each element in these materials has been calculated from the critical energy deficit. Different binding energies due to different surface conditions can be seen. The binding energies of pure metals are very closed to the values of cohesive energy from the standard table. From these results, we believe that the binding energy of surface atoms can really be measured by this system and from well defined crystal surfaces and atomic sites at low temperatures.

2. INSTRUMENTATION

A pulsed-laser time-of-flight atom-probe was built in 1983[4]. Since then some improvements have been made. The whole system is shown in Fig. 1. The major object of the

improvements of the system is to have a high energy resolution in energy distribution measurements. From the equation

$$E=(1/2)Mv^2=(1/2)M(L/t)^2 ,$$

where E is the kinetic energy of the field emitted ions, M is the ion mass, L is the flight path length and t is the time of flight. So the energy resolution $\Delta E/E$ depends on $\Delta M/M$, $\Delta t/t$, $\Delta L/L$. Usually we know the ion masses accurately, so that the energy resolution is limited by $\Delta t/t$ and $\Delta L/L$ only. The time uncertainty Δt comes mainly from two sources. They are the time resolution of the flight-time measurement devices and the time width of the field desorption. The path uncertainty ΔL is the maximum difference in the flight path lengths of ions taking the shortest and longest possible routes. By placing the tip at the focal point of the einzel lens, the ions will travel along the axial direction after passing through the einzel lens; thus ΔL can be minimized. By expanding the flight path to 7.78 meters, L and t are both enlarged, so $\Delta L/L$ and $\Delta t/t$ can be minimized.

It is desired to have the entire flight path free of field in order to have a free flight for the traveling ions. The electric fields in the system are restricted to small regions, either between the tip and the grounded aluminum cone or in front of the ion detector at the end of the flight tube. The effect from the earth magnetic field is shielded by wraping the entire flight path by high-μ metals. In order to achieve the highest energy resolution, it is necessary to use the timer with a highest resolution. With the use of an IEEE interface card within an IBM PC XT and with the LeCroy 8901 and 4204 TDC having 156 ps time resolution, the energy resolution is better than 1/50,000. A stable high power supply is also needed for supplying a constant potential to the field emitted ions. A KEITHLEY 196 system digital multifunction meter is also used with 6 digits voltage resolution to read out the tip voltage via a voltage divider of 1/10,000 of real voltages.

3. CALIBRATION OF THE SYSTEM

To achieve an adequate accuracy for the binding energy measurement, a very careful calibration of the system is necessary. This is done with field desorbed inert gas ions. The critical energy deficits of these ions are given by $E_C = I - \phi$, where the ionization energy I are known from spectroscopic data to better than 0.01 eV. Since in a ToF measurement of the ion energy distributions, ions spend most of its flight times in the flight-tube, a contact potential correction requires that the emitter work function ϕ be replaced with the average work function of the flight tube. We find a value of 4.5 ±0.1 eV [6] gives the best result.

3.1 The Flight-Path and Time Delay Constants

In the time-of-flight measurement, the kinetic energy of the field emitted ions is

$$E_k = (1/2)Mv^2 = (1/2)M(L/t)^2 = neV - E_C , \qquad (3\text{-}1)$$

where M is the ion mass, L is the flight path length, and V is the applied voltage. The mass to charge ratio is

$$M/n = C(V - E_C/ne)(t_0+\delta)^2 , \qquad (3\text{-}2)$$

$$C = 2e/L^2 , \quad t = t_0 + \delta ,$$

where C is the flight path constant, t_0 is the onset flight time and δ is the time delay constant. The flight path constant C is determined by the flight path length, and the time delay constant comes from the electronic system including the response time of the electronic devices and the transmission time through the cables. Since the ionic masses of the gas ions are known to an accuracy of eight significant figures or better[7], and the critical energy deficit from theoretical calculation are known quite well, it is possible for us to derive C and δ by measuring t_0 as a function of V as follows:

$$t_0 = (1/C)^{1/2}((M/n)/(V - E_C/ne))^{1/2} - \delta ,$$

and by taking a linear regression of t_0 vs X according to

$$t_0 = KX - \delta$$

where

$$K = (1/C)^{1/2} \; ; \; X = ((M/n)/(V - E_C/ne))^{1/2} .$$

The slope of the plot is the value K, and the intercept of the plot with the X-axis is the time delay constant δ. But since a graphical method cannot achieve the desired precision, a numerical method must be used. Table 1 lists the data. The best linear fit gives C = 0.003187805 u/ms/KV, and the time delay δ = 20.1 ns. The excellent linearity of this plot is exhibited in the value of the coefficient of correlation 0.999 999 996, almost identical to 1.

3.2 Precision Measurement of Ionic Masses and Critical Energy Deficits

The precision measurements of ionic masses and the critical energy deficits of gaseous and metal ions are listed in Table 2. The differences between measured ion masses and the values from the standard table are less than or about 0.001 amu for all ions. The average difference between measured critical energy deficits and the theoretical calculated critical energy deficits is less than or about 0.1 eV. As the energies usually average above 5 KV, the energy resolution of 1/50,000 has been achieved.

4. RESULTS AND DISCUSSIONS

Consider an atom at a kink site of a crystal; the energy needed to remove this atom to vacuum level is the binding energy. The energy needed for an atom to be ionized is the ionization energy. But the total energy needed will be smaller by nø since the released electrons from the atom are returned to the crystal. n is the charge state of the ion, and the ø is the work function of the crystal. This energy is the critical energy deficit for field evaporate n-fold charged ions[8] .

$$E_C = \Lambda + I - n\phi \qquad (4\text{-}1)$$

where Λ is the binding energy, I is the total ionization energy. So the kink sites specific binding energy Λ of the surface atoms can be determined by

$$\Lambda = E_C - I + n\phi . \qquad (4\text{-}2)$$

Since E_C is derived, based on the Born-Haber energy cycle, from the difference of the potential energy applied and the kinetic energy measured, the effect of high field will not come into this calculation if we neglect the activation energy which is on the order of 0.1 eV.

Experimental data are listed in Table 3. For the pure metals, W(110) and Rh(100), the critical energy deficits we obtained are 45.36 eV for W and 22.46 eV for Rh. Thus the binding energies are 8.88 eV for W and 5.92 eV for Rh. Compared to the data derived from thermodynamic methods as listed in the standard table, the binding energies are 8.66 eV and 5.75 eV for W and Rh respectively[9]. Our experiment thus shows that the binding energy of kink site atoms of the W(110) plane is equal to the bulk binding energy of W. The same applies to the Rh(100) plane with bulk Rh.

For Pt-44.2 % Rh alloy, from the onset flight times for these ions, the critical energy deficits are found to be 19.98 eV for Rh^{2+} and 23.20 eV for Pt^{2+}. Using eq. (4-2) and the ionization energies from the standard table[10], we find that the binding energies of Rh and Pt atoms on the (100) planes of this Pt-Rh alloy are 3.45 eV and 4.64 eV respectively. The binding energies of Rh atoms in pure Rh and Pt atoms in pure Pt are 5.75 eV and 5.85 eV respectively. Thus the binding energies of Rh and Pt atoms on the PtRh(100) surface are almost 25 to 30 percent less than the binding energies in their own respective lattices. In Fig. 2, we show two distributions of Rh^{2+}, one from pure Rh and one from Pt-Rh alloy, the onset flight times are obviously separated.

The first ionization energy of the Ga atom is 6.0 eV; therefore the binding energy is 1.69 eV for Ga^{+} from a GaAs(111) surface. It is lower than the binding energy of either Ga from pure Ga of 2.81 eV or GaAs from GaAs of 5.57 eV [11-14]. In pulsed-laser stimulated field evaporation of semiconductors, the critical energy deficits are always found to be much lower than those calculatedby eq. (4.2). We believe thatphoto-excitations occur in the evaporation.

5. CONCLUSIONS

The binding energies of kink site atoms of single element metals are shown to be the same as the cohesive energy of these metals reported in the standard table in which the data was obtained by high temperature methods. This means that the cohesive energy of a solid and site specific binding energy of surface atoms can be obtained from solids of well-defined crystal structures at low temperatures. Any deviation of binding energies from the standard table can be proved to be due to changes of surface atomic configurations. The kink-site binding energies of Rh or Pt on Pt-44.2 % Rh alloy (100) plane are less than the binding energies of Rh or Pt in pure Rh or Pt metal. For semiconductors, further consideration of photoexcitation effect is needed.

This method can be used to derive the binding energy of atoms adsorbed on different crystal planes in the near future. This is vital information for a fundamental understanding of the energetics of many surface atomic processes which govern crystal growth, chemical reaction, and many other surface phenomena. Hence this study opens up a new field to study the basic physics of surface science.

REFERENCES

1. See for examples: V. L. Moruzzi, J. F. Janok and A. R. Williams,Calculated Electronic Properities of Metals (Pregamon, N. Y. 1978); M. T. Yin and M. L. Cohen, Phys. Rev. B26, 5668 (1982); R. Needs and R. M. Martin, Phys. Rev. B30, 5372 (1984); R. Biswas and D. R. Hamann, Phys. Rev. Lett. 55, 2001 (1985); J. A. Moriaty, Phys. Rev. Lett. 55, 1502 (1985).
2. C. Kittel,"Introduction of Solid State Physics" 5th ed., chapter 3.

3. See for examples: E. W. Muller and T. T. Tsong, Field Ion Microscopy, Principles and Applications, Elsevier, New York (1969); also Prog. Surf. Sci. 4, 1 (1973).
4. T. T. Tsong, T. J. Kinkus and S. B. McLane, 31st Field Emission Symp. 1983.
5. See for example: T. T. Tsong, Y. Liou and S. B. McLane, Rev. Sci. Instrum. 55, 1246 (1984).
6. For principles of the method see T. T. Tsong, Phys. Rev. B30, 4946 (1984); Surf. Sci. 177, 593 (1986).
7. See Tables of Isotopes, C. M. Lederer and V. S. Shirley eds. (Wiley, New York 1978).
8. T. T. Tsong, W. A. Schmidt, and O. Frank, Surf. Sci. 65, 109 (1977).
9. L. Brewer, Lawrence Berkeley Laboratory Report No. 3720 (1975).
10. C. E. Moore, Atomic Energy Levels (NBS, Washington D. C. 1971).
11. M. Hansen and K. Anderko, "Constitution of Binary Alloys", 2nd ed., McGraw-Hill 1958.
12. W. B. Pearson, "A Handbook of Lattice Spacings and Structures of Metals and Alloys", Pergamon Press, 1967.
13. Ed. by T. B. Massalski et al, "Binary alloys Phase Diagrams", National Bureau of Standards data, 1986.
14. Compiled by B. R. Pamplin in "Handbook of Chemistry and Physics", CRC Press, 66th ed.,1985.

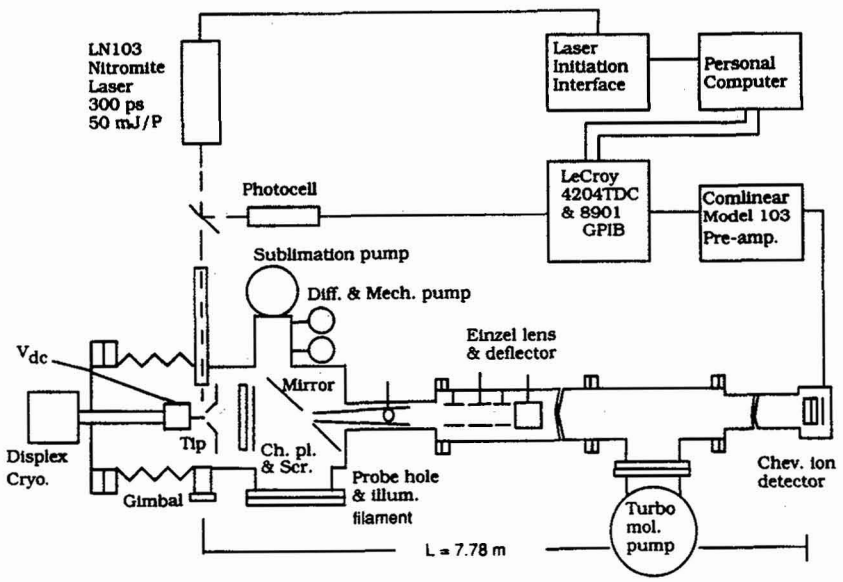

Fig.1. Schematic diagram of the pulsed-laser time-of-flight atom-probe field-ion microscope.

TABLE 1. Datas for various gas species.

Ionic Species Mass, $\Delta E_C/n$	V (kV)	$[M/(V-\Delta E_C/e)]^{1/2}$ (amu/KV)$^{1/2}$	T_0 (μs)
He^+ 4.002054 amu, 0.0201 KV	2	1.421 738 894	25.1630
	2.5	1.270 352 913	22.4810
	3	1.158 885 913	20.5060
	3.5	1.072 403 173	18.9730
	4	1.002 779 373	17.7400
	4.5	0.945 164 306	16.7200
	5	0.896 460 505	15.8560
	5.5	0.854 584 783	15.1150
	6	0.818 077 619	14.4690
	6.5	0.785 881 961	13.8990
	7	0.757 210 925	13.3915
	7.5	0.731 465 043	12.9355
	8	0.708 178 516	12.5230
	8.5	0.686 983 184	12.1475
	9	0.667 583 696	11.8040
Ne^+ 19.99189 amu, 0.017 KV	4	2.240 380 446	39.6590
	5	2.003 002 462	35.4530
	6	1.827 963 103	32.3560
	6.5	1.756 058 243	31.0820
	7	1.692 021 611	29.9490
	7.5	1.634 515 541	28.9305
N_2^+ 28.005599 amu, 0.0111 KV	3.5	2.833 206 613	50.1580
	4	2.649 694 831	46.9120
Ar^+ 39.961834 amu, 0.0113 KV	3.5	3.384 471 748	59.9220
	4	3.165 242 724	56.0440

Best fit data : $\delta = 20.1$ ns, $C = 0.003187805$. Linearity : $\gamma^2 = 0.999\,999\,996$

TABLE 2. Ionic masses and critical energy deficits of gas ions experiments

Ionic Species	Ion Mass (amu)	Measured Ion Mass, (amu)	ΔM	$\Delta E_C/n$ (eV)	Measured $\Delta E_C/n$,(eV)
He^+	4.002054	4.002061±0.00034	0.0000007±0.00034	20.1	20.09±0.38
Ne^+	19.99189	19.99154±0.0023	0.00035±0.0023	17	16.97±0.45
Ar^+	39.961834	39.962814±0.0034	0.00098±0.0034	11.3	11.41±0.33
N^{2+}	28.005599	28.005723±0.002	0.000124±0.0025	11.1	11.14±0.53
Rh^{2+}	51.452201	51.4527358±0.0003	0.00053±0.00061	11.15	11.23±0.04
W^{3+}					
182	60.6489	60.64970±0.0011			15.14±0.16
183	60.9828	60.98455±0.0.0031			15.37±0.50
184	61.3166	61.31658±0.0012			15.10±0.18
186	61.9842	61.98267±0.0022	0.0012±0.00068	15.1	14.88±0.47

TABLE 3. Critical energy deficits for various metal ions.

Ionic Species	Crystal Plane	$\Delta E_C/n$ (eV)	Measured $\Delta E_C/n$,(ev)	Λ (eV)	Measured Λ, (eV)
W^{3+}	W(110)	15.1	15.12±0.17	5.75	5.92
Rh^{2+}	Rh(100)	11.15	11.23±0.04	8.66	8.88
Rh^{2+}	Pt-Rh(100)		9.99	5.75	3.45
Pt^{2+}	Pt-Rh(100)		11.60±0.013	5.85	4.64
Ga^+	GaAs(111)		3.19±0.15	2.81	1.69

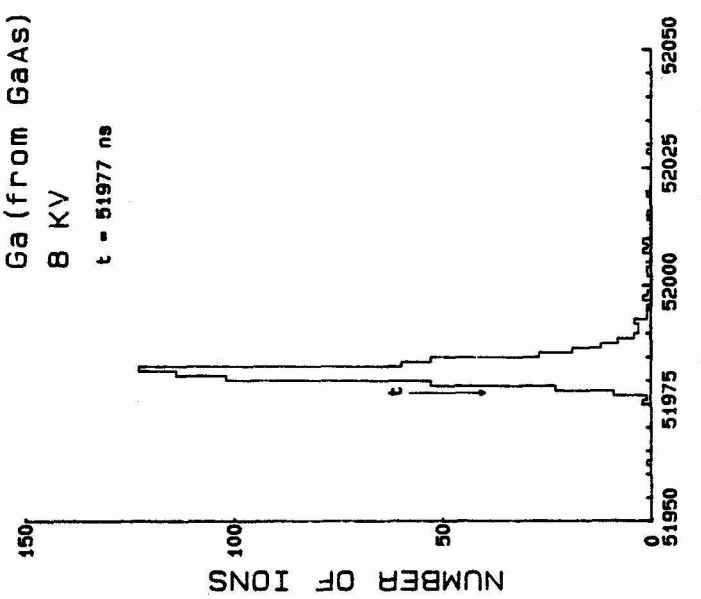

Fig. 3. The energy distribution of Ga^{+}(69) from GaAs(111) surface.

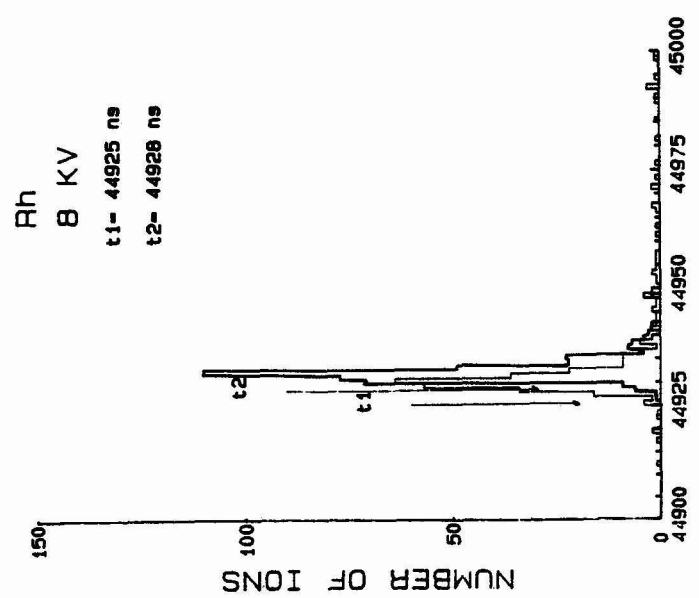

Fig. 2. Two energy distributions of Rh^{2+} from pure Rh and PtRh alloy at 8 KV. Two onset flight times, t_1 from PtRh and t_2 from Rh, are 3 ns different